bioRxiv preprint doi: https://doi.org/10.1101/683839; this version posted June 27, 2019. The copyright holder for this preprint (which was not certified by peer review) is the author/funder. All rights reserved. No reuse allowed without permission.

Modeling bacteria-based therapy in tumor spheroids

Pietro Mascheroni[a], Michael Meyer-Hermann[a,b,c,*], Haralampos Hatzikirou[a,*]

[a] *Braunschweig Integrated Centre of Systems Biology and Helmholtz Centre for Infection Research, Braunschweig, Germany.*
[b] *Centre for Individualized Infection Medicine, Hannover, Germany.*
[c] *Institute for Biochemistry, Biotechnology and Bioinformatics, Technische Universität Braunschweig.*

Abstract

Tumor-targeting bacteria elicit anticancer effects by infiltrating hypoxic regions, releasing toxic agents and inducing immune responses. As the mechanisms of action of bacterial therapies are still to be completely elucidated, mathematical modeling could aid the understanding of the dynamical interactions between tumor cells and bacteria in different cancers. Here we propose a mathematical model for the anti-tumor activity of bacteria in tumor spheroids. We consider constant infusion and time-dependent administration of bacteria in the culture medium, and analyze the effects of bacterial chemotaxis and killing rate. We show that active bacterial migration towards tumor hypoxic regions is necessary for successful spheroid infiltration and that intermediate chemotaxis coefficients provide the smallest spheroid radii at the end of the treatment. We report on the impact of the killing rate on final spheroid composition, and highlight the emergence of spheroid size oscillations due to competing interactions between bacteria and tumor cells.

Keywords: Cancer, Bacterial therapy, Mixture theory, Chemotaxis, Space competition

*Correspondence:
mmh@theoretical-biology.de (M.M.H.);
haralampos.hatzikirou@helmholtz-hzi.de (H.H.)

bioRxiv preprint doi: https://doi.org/10.1101/683839; this version posted June 27, 2019. The copyright holder for this preprint (which was not certified by peer review) is the author/funder. All rights reserved. No reuse allowed without permission.

1. Introduction

Cancers display huge variability between different patients and even in the same patient. Nonetheless, cancer cells share a finite set of hallmarks such as sustained proliferation, invasion and metabolic reprogramming, which shape their behavior in solid tumors (Hanahan and Weinberg, 2011). Among other hallmarks, tumor cells are known to recruit new blood vessels to sustain their proliferation, in a process known as *tumor angiogenesis* (Folkman, 1971). This neovasculature is generally altered in terms of architecture and morphology of the vessels, leading to poor perfusion of certain areas of the tumor (Carmeliet and Jain, 2000). Hypoxic regions are thus created and maintained during tumor development, concurring to the progression of cancer cells towards malignant phenotypes (Vaupel and Mayer, 2007). Moreover, low nutrient levels can lead to cell quiescence, a situation in which tumor cells delay metabolic activities and become less sensitive to standard chemotherapies (Challapalli et al., 2017). Such hypo-perfused areas are generally associated with poor patient outcome but, on the other hand, could be exploited for tumor targeting (Wilson and Hay, 2011). The same hypoxic areas provide indeed a niche for bacteria to colonize the tumor and exert a therapeutic action (Forbes, 2010; Zhou et al., 2018). The use of bacteria for cancer therapy dates back hundreds of years, with doctors reporting tumor regression in several patients (Kramer et al., 2018). However, such treatments also caused some fatalities and the limited understanding of the mechanisms of action of these therapies shifted research efforts towards other strategies - especially radiotherapy (Kramer et al., 2018). In the last few years the use of live bacteria for cancer treatment has gained new interest, and several bacterial strains have been tested in animal models and even advanced to clinical trials (Torres et al., 2018). Nevertheless, clinical development of such therapies is still facing significant issues due to infection-associated toxicities and incomplete knowledge of infection dynamics (Kramer et al., 2018; Zhou et al., 2018).

Mathematical modeling emerges as a promising candidate to assist the understanding of the mechanism of action of bacterial therapy in cancer. Mathematical models have been applied in the context of cancer to elucidate its progression and treatment (Byrne, 2010; Altrock et al., 2015). The authors in (Kasinskas and Forbes, 2006) performed experiments to quantify the accumulation of bacteria in an *in vitro* tumor tissue. Using fluorescent microscopy they measured the accumulation of *Salmonella typhimurium* into

bioRxiv preprint doi: https://doi.org/10.1101/683839; this version posted June 27, 2019. The copyright holder for this preprint (which was not certified by peer review) is the author/funder. All rights reserved. No reuse allowed without permission.

cylindroids of different size. Their results were fitted to a mathematical model quantifying bacterial growth and infiltration in the cellular aggregate, showing that bacteria accumulate for longer times in larger cylindroids. Using a similar approach in a different *in vitro* setting, another group analyzed the impact of bacterial motility on tumor accumulation (Toley and Forbes, 2011). They considered different bacterial strains belonging to *Salmonella typhimurium* and *Escherichia coli*, and observed that only the most motile of them was able to colonize the tumor at low inoculation densities. Through a mathematical model informed by the experiments the authors showed that bacterial dispersion provides deeper infiltration in the tumor, whereas bacterial growth leads to increased bacterial densities. A cytotoxic protein in *Escherichia coli* was cloned to investigate its effects on tumors as discussed in (Jean et al., 2014). The authors of the article showed that bacteria were able to secrete this protein when injected in tumors, leading to cell death and tumor volume reduction. The authors measured the distribution of the protein in the tissue and observed a large necrotic area following treatment. They introduced a mathematical model for molecular transport and showed that the protein efficacy in killing cancer cells primarily depends on the colony size and rate of production. More recently, a mathematical model for immune recruitment in tumors by bacterial infections was proposed in (Hatzikirou et al., 2017). Calibrated on mice data, the model showed that increasing bacterial loads does not always produce long-term tumor control, suggesting the existence of optimal bacterial loads depending on tumor size. In addition, the model predicted that the combined effect of intermediate bacterial loads and low administration of a proinflammatory cytokine may lead to improved therapeutic outcomes. The infiltration of nanoparticles and bacteria in *in vitro* tumors was analyzed in (Suh et al., 2018). Through mathematical modeling the authors showed that bacteria display higher effective diffusivities compared to nanoparticles, suggesting their use as drug vectors in future cancer treatments. Notably, they validated their modeling procedure with experiments using tumor spheroids. The latter are aggregates of tumor cells (approximately spherical) that can be grown *in vitro*, mimicking the growth dynamics and generation of hypoxic areas in small avascular tumors.

Here we describe a mathematical model for bacteria-based cancer therapy within tumor spheroids. The model is formulated in the context of mixture theory, a continuum theory with a long history of applications to biological problems - see for example Ambrosi and Preziosi (2002); Breward et al. (2001, 2002, 2003); Byrne and Preziosi (2003); Chaplain et al. (2006); Preziosi and

bioRxiv preprint doi: https://doi.org/10.1101/683839; this version posted June 27, 2019. The copyright holder for this preprint (which was not certified by peer review) is the author/funder. All rights reserved. No reuse allowed without permission.

Tosin (2009) and the recent reviews of Siddique et al. (2017); Pesavento et al. (2017). Our aim is to evaluate the impact of bacterial chemotaxis and anti-tumor activity on spheroid size and composition. We consider two regimes, i.e. a constant infusion of bacteria in the culture medium and an administration after the spheroid is fully established. We describe the effects of the treatment on the behavior of the spheroid constituents, e.g. tumor cells and bacteria volume fractions, at different time points and over the spheroid radius.

The remainder of the paper is organized as follows. In Section 2 we describe the mathematical model and its derivation. In Section 3 we present model results, first focusing on continuous infusion of bacteria and then analyzing time-controlled bacterial administration. Finally, in Section 4 we discuss the biological implications of the results and suggest new research directions.

2. Mathematical model

We propose a mathematical model describing the impact of bacterial cells on tumor spheroid growth. The model is based on mixture theory, following the approach discussed in Preziosi (2003); Byrne (2012). Specifically, we follow the derivation in Boemo and Byrne (2019) which deals with a mixture model for macrophage-based therapies in tumor spheroids. We describe the tumor as being composed of three main constituents (or *phases* in the language of mixture theory): tumor cells (TCs), bacteria and extracellular material. The variables referring to these quantities will be identified by the indexes c, b and f, respectively. The model equations are derived by applying conservation of mass and linear momentum to each phase. Then, we close the model by imposing suitable constitutive assumptions regarding the material properties of the phases and their interaction terms.

The balance of mass for each phase reads:

$$\partial_t \phi_{\mathrm{i}} + \mathrm{div}\,(\phi_{\mathrm{i}} \boldsymbol{v}_{\mathrm{i}}) = S_{\mathrm{i}}, \tag{1}$$

in which ϕ_{i}, $\boldsymbol{v}_{\mathrm{i}}$ and S_{i} are the volume fraction, velocity and mass exchange term related to the i-th phase (i = c, b, f). Note that Equation (1) implicitly assumes that the phases have the same constant mass density. In the following we will also assume that the mixture is closed with respect to mass, so that mass can only be converted from one phase to the other, i.e. $S_{\mathrm{f}} = -S_{\mathrm{c}} - S_{\mathrm{b}}$.

bioRxiv preprint doi: https://doi.org/10.1101/683839; this version posted June 27, 2019. The copyright holder for this preprint (which was not certified by peer review) is the author/funder. All rights reserved. No reuse allowed without permission.

In mixture theory velocity fields are determined by considering the mechanical response of the phases to mutual interactions. Neglecting inertial effects, as usually done for growth phenomena (Preziosi, 2003; Byrne, 2012), the balance of linear momentum can be written as:

$$\mathrm{div}\left(\boldsymbol{\sigma}_{\mathrm{i}}\right) + \sum_{\mathrm{i}\neq\mathrm{j}} \boldsymbol{m}_{\mathrm{ij}} + p\,\mathrm{grad}\left(\phi_{\mathrm{i}}\right) = \boldsymbol{m}_{\mathrm{i}}. \tag{2}$$

Here $\boldsymbol{\sigma}_{\mathrm{i}}$ is the partial stress tensor of the i-th phase, $\boldsymbol{m}_{\mathrm{ij}}$ represent the forces exerted on the i-th phase by the j-th phase, and $\boldsymbol{m}_{\mathrm{i}}$ describes an external force acting on the i-th phase (i, j = c, b, f). Note that, for the action-reaction principle, $\boldsymbol{m}_{\mathrm{ij}} = -\boldsymbol{m}_{\mathrm{ji}}$. Finally, the terms $p\,\mathrm{grad}\left(\phi_{\mathrm{i}}\right)$ represent interfacial effects between phases, with p being the interfacial pressure (Byrne, 2012). In this modeling framework, p emerges as a Lagrange multiplier due to the saturation constraint

$$\sum_{\mathrm{i}=\mathrm{c,b,f}} \phi_{\mathrm{i}} = 1, \tag{3}$$

meaning that we assume that there are no empty spaces within the mixture (Preziosi, 2003; Byrne, 2012).

We conclude the set of governing laws by stating an equation for the normalized nutrient concentration n in the mixture, i.e. the tumor:

$$\partial_t n = D_{\mathrm{n}}\mathrm{div}\left(\mathrm{grad}\, n\right) + S_{\mathrm{n}}, \tag{4}$$

in which D_{n} is the nutrient diffusion coefficient and S_{n} represents the nutrient mass exchange with the model phases. In the following we will consider a single nutrient, i.e. oxygen.

2.1. Constitutive relationships

We close the model by selecting suitable constitutive assumptions. First, we assume that the interaction terms m_{ij} depend linearly on the relative phase velocities (Preziosi, 2003; Byrne, 2012):

$$\boldsymbol{m}_{\mathrm{ij}} = -\mu\phi_{\mathrm{i}}\phi_{\mathrm{j}}\left(\boldsymbol{v}_{\mathrm{i}} - \boldsymbol{v}_{\mathrm{j}}\right), \tag{5}$$

with the same linearity constant μ for all the phases (i = c, b, f). We consider only a single external force $\boldsymbol{m}_{\mathrm{b}}$ acting on bacteria. This term describes bacteria chemotaxis following spatial hypoxic gradients and models

bioRxiv preprint doi: https://doi.org/10.1101/683839; this version posted June 27, 2019. The copyright holder for this preprint (which was not certified by peer review) is the author/funder. All rights reserved. No reuse allowed without permission.

active cell migration towards waste products from dying cancer cells (Forbes, 2010; Toley and Forbes, 2011). We assume a linear relationship,

$$\boldsymbol{m}_{\mathrm{b}} = \phi_{\mathrm{b}}\chi_{\mathrm{b}}\mathrm{grad}\, n, \tag{6}$$

in which χ_{b} describes the strength of chemoattraction.

Following Breward et al. (2001, 2002); Byrne (2012); Boemo and Byrne (2019) we consider the phases as inviscid fluids and associate an interfacial pressure to each of them. For simplicity, we take the pressure in the extracellular material to be equal to that in the fluid surrounding the spheroid, p. The partial stress tensors in Equation (2) are defined such that the interfacial pressure of each phase is given by the pressure in the extracellular material plus a correction term, specific to its phase (Boemo and Byrne, 2019):

$$\boldsymbol{\sigma}_{\mathrm{f}} = -p\boldsymbol{I}, \tag{7}$$

$$\boldsymbol{\sigma}_{\mathrm{b}} = -(p + \pi_{\mathrm{b}})\boldsymbol{I}, \tag{8}$$

$$\boldsymbol{\sigma}_{\mathrm{c}} = -(p + \pi_{\mathrm{c}})\boldsymbol{I}, \tag{9}$$

where $\boldsymbol{I}$ is the identity tensor. The ratio π_{i}/μ characterizes the movement of the i-th phase in the mixture and is generally identified as the phase motility coefficient D_{i} (i = c, b) (Boemo and Byrne, 2019). In the following we will also define $\chi = \chi_{\mathrm{b}}/\mu$ as the bacterial chemotactic coefficient.

To formulate the mass exchange terms in Equations (1) and (4) we assume the following assumptions:

A1 TCs proliferate when oxygen is available. As soon as the latter decreases below a critical threshold, they stop proliferating and start necrosis (Chaplain et al., 2006; Gerlee and Anderson, 2007; Agosti et al., 2018).

A2 Bacteria compete with TCs for space and exert an anti-tumor effect by a variety of mechanisms (e.g. by realising toxins and therapeutic agents, or stimulating an immune response). (Forbes, 2010; Osswald et al., 2015; Torres et al., 2018; Zhou et al., 2018).

A3 Bacteria die when oxygen is above a critical threshold and thrive in hypoxic conditions (*anaerobic* bacteria) (Toley and Forbes, 2011; Phaiboun et al., 2015; Osswald et al., 2015).

bioRxiv preprint doi: https://doi.org/10.1101/683839; this version posted June 27, 2019. The copyright holder for this preprint (which was not certified by peer review) is the author/funder. All rights reserved. No reuse allowed without permission.

A4 TCs consume oxygen provided by the culture medium (Matzavinos et al., 2009; Grimes et al., 2014).

The resulting mass exchange terms read:

$$S_{\mathrm{c}} = \gamma_{\mathrm{c}}\phi_{\mathrm{c}}\phi_{\mathrm{f}}\mathcal{H}\left(\frac{n}{n_{\mathrm{cr}}} - 1\right) - \delta_{\mathrm{c}}\phi_{\mathrm{c}}\mathcal{H}\left(1 - \frac{n}{n_{\mathrm{cr}}}\right) - \kappa\phi_{\mathrm{c}}\phi_{\mathrm{b}}, \tag{10}$$

$$S_{\mathrm{b}} = \gamma_{\mathrm{b}}\phi_{\mathrm{b}}\phi_{\mathrm{f}}\mathcal{H}\left(1 - \frac{n}{n_{\mathrm{cr}}}\right) - \delta_{\mathrm{b}}\phi_{\mathrm{b}}\mathcal{H}\left(\frac{n}{n_{\mathrm{cr}}} - 1\right), \tag{11}$$

$$S_{\mathrm{n}} = -\delta_{\mathrm{n}}\phi_{\mathrm{c}}n. \tag{12}$$

Here γ_{i} and δ_{i} are the proliferation and death rate of the i-th phase respectively ($\mathrm{i} = \mathrm{c}, \mathrm{b}$), whereas δ_{n} is the oxygen consumption rate. We indicate with $\mathcal{H}(\cdot)$ a smooth version of the step function, and with n_{cr} the critical oxygen value below which hypoxic conditions develop. Finally, we do not consider a specific form for the anti-tumor effect of bacteria and introduce an effective TC killing rate κ in the equation for S_{c}.

2.2. Spherical symmetry, initial and boundary conditions

In the following we will be interested in the case of tumor spheroids, for which the assumption of spherical symmetry applies. Therefore, we enforce the problem symmetry and rewrite the equations in terms of one-dimensional, radially symmetric spherical coordinates. We introduce the radial coordinate r defining the radial distance from the center of the spheroid. Recasting Equation (1) in spherical symmetry, after imposing the saturation constraint in Equation (3), gives:

$$v_{\mathrm{c}}\phi_{\mathrm{c}} + v_{\mathrm{b}}\phi_{\mathrm{b}} + v_{\mathrm{f}}\phi_{\mathrm{f}} = 0, \tag{13}$$

in which v_{i} is the radial velocity of the i-th phase ($\mathrm{i} = \mathrm{c}, \mathrm{b}, \mathrm{f}$). Substituting Equations (5), (7)-(9) and (13) in Equation (2) we obtain for the radial velocities:

$$v_{\mathrm{c}} = D_{\mathrm{b}}\frac{\partial\phi_{\mathrm{b}}}{\partial r} + D_{\mathrm{c}}\left(1 - \frac{1}{\phi_{\mathrm{c}}}\right)\frac{\partial\phi_{\mathrm{c}}}{\partial r} + \chi\phi_{\mathrm{b}}\frac{\partial n}{\partial r}, \tag{14}$$

$$v_{\mathrm{b}} = D_{\mathrm{b}}\left(1 - \frac{1}{\phi_{\mathrm{b}}}\right)\frac{\partial\phi_{\mathrm{b}}}{\partial r} + D_{\mathrm{c}}\frac{\partial\phi_{\mathrm{c}}}{\partial r} - \chi\left(1 - \phi_{\mathrm{b}}\right)\frac{\partial n}{\partial r}, \tag{15}$$

bioRxiv preprint doi: https://doi.org/10.1101/683839; this version posted June 27, 2019. The copyright holder for this preprint (which was not certified by peer review) is the author/funder. All rights reserved. No reuse allowed without permission.

after summing over the phases in Equation (2) to express p as a function of the other model quantities (Boemo and Byrne, 2019). Substituting Equations (14)-(15) in (1) and rewriting the system in spherical symmetry leads to

$$\frac{\partial \phi_{\mathrm{c}}}{\partial t} = \frac{1}{r^2}\frac{\partial}{\partial r}\left\{r^2\left[D_{\mathrm{c}}\left(1-\phi_{\mathrm{c}}\right)\frac{\partial \phi_{\mathrm{c}}}{\partial r} - D_{\mathrm{b}}\phi_{\mathrm{c}}\frac{\partial \phi_{\mathrm{b}}}{\partial r} - \chi\phi_{\mathrm{c}}\phi_{\mathrm{b}}\frac{\partial n}{\partial r}\right]\right\} + S_{\mathrm{c}}, \tag{16}$$

$$\frac{\partial \phi_{\mathrm{b}}}{\partial t} = \frac{1}{r^2}\frac{\partial}{\partial r}\left\{r^2\left[D_{\mathrm{b}}\left(1-\phi_{\mathrm{b}}\right)\frac{\partial \phi_{\mathrm{b}}}{\partial r} - D_{\mathrm{c}}\phi_{\mathrm{b}}\frac{\partial \phi_{\mathrm{c}}}{\partial r} + \chi\phi_{\mathrm{b}}\left(1-\phi_{\mathrm{b}}\right)\frac{\partial n}{\partial r}\right]\right\} + S_{\mathrm{b}}, \tag{17}$$

$$\frac{\partial n}{\partial t} = \frac{1}{r^2}\frac{\partial}{\partial r}\left(r^2 D_{\mathrm{n}}\frac{\partial n}{\partial r}\right) + S_{\mathrm{n}}. \tag{18}$$

Note that we do not solve for ϕ_{f} since it can be obtained as $\phi_{\mathrm{f}} = 1-\phi_{\mathrm{c}}-\phi_{\mathrm{b}}$ through Equation (3).

We model growth of the spheroid as a free-boundary problem, in which the outer tumor radius $r = R(t)$ moves with the same velocity as the TC phase,

$$\frac{dR}{dt} = v_{\mathrm{c}}(R,t). \tag{19}$$

Finally, we define a set of boundary and initial conditions to close the differential problem in Equations (16)-(18). Due to the problem symmetry no-flow boundary conditions are enforced at the spheroid center, whereas we fix the values of TC volume fraction, bacterial volume fraction and normalized nutrient concentration on the spheroid boundary:

$$\partial_r \phi_{\mathrm{c}} = \partial_r \phi_{\mathrm{b}} = \partial_r n = 0, \quad r = 0 \tag{20}$$

$$\phi_{\mathrm{c}} = \phi_{\mathrm{c0}}, \quad \phi_{\mathrm{b}} = \phi_{\mathrm{b0}}, \quad n = 1, \quad r = R(t). \tag{21}$$

In the following, we assume a uniform initial tumor volume fraction $\phi_{\mathrm{c0}} = 0.8$ across the spheroid (Byrne and Preziosi, 2003) and consider a small value for the bacterial volume fraction at the spheroid outer radius, i.e. $\phi_{\mathrm{b0}} = 0.01$. Regarding the initial conditions, we consider a spheroid devoid of bacteria and displaying a uniform TC volume fraction and nutrient concentration over its radius:

$$\phi_{\mathrm{c}}(r,0) = \phi_{\mathrm{c0}}, \quad \phi_{\mathrm{b}} = 0, \quad n = 1. \tag{22}$$

Finally, we prescribe an initial spheroid radius, i.e. $R(0) = 150\,\mu\mathrm{m}$.

bioRxiv preprint doi: https://doi.org/10.1101/683839; this version posted June 27, 2019. The copyright holder for this preprint (which was not certified by peer review) is the author/funder. All rights reserved. No reuse allowed without permission.

Parameter	Value	Description	Reference
D_c	$8.64 \times 10^{-2}\,\mathrm{mm^2 d^{-1}}$	TC motility coefficient	(Chaplain et al., 2006)
γ_c	$1\,\mathrm{d^{-1}}$	TC proliferation rate	(Chaplain et al., 2006)
n_{cr}	0.6	Critical oxygen concentration	(Gerlee and Anderson, 2007)
δ_c	$0.5\,\mathrm{d^{-1}}$	TC death rate	(Martínez-González et al., 2012)
D_b	$5 \times 10^{-2}\,\mathrm{mm^2 d^{-1}}$	Bacterial motility coefficient	(Toley and Forbes, 2011)
γ_b	$15\,\mathrm{d^{-1}}$	Bacterial proliferation rate	(Gibson et al., 2018)
δ_b	$0.24\,\mathrm{d^{-1}}$	Bacterial death rate	(Phaiboun et al., 2015)
D_n	$1 \times 10^2\,\mathrm{mm^2 d^{-1}}$	Oxygen diffusion coefficient	(Matzavinos et al., 2009)
δ_n	$8.64 \times 10^3\,\mathrm{d^{-1}}$	Oxygen consumption rate	(Colombo et al., 2015)
χ	$[0, 8.64 \times 10^{-1}]\,\mathrm{mm^2 d^{-1}}$	Bacterial chemotactic coefficient	estimated
κ	$[0, 10]\,\mathrm{d^{-1}}$	Bacterial killing rate	model specific

Table 1: Summary of the parameter estimates used to carry out the model simulations.

2.3. Parameter estimation

The parameters used in the model simulations are reported in Table 1. As we do not focus on a specific cell line we use the generic estimate for TC motility and proliferation rate reported in (Chaplain et al., 2006). For the critical oxygen concentration, below which cells experience hypoxic conditions, we take a value similar to the one in (Gerlee and Anderson, 2007; Agosti et al., 2018). Also, we select the TC death rate in accordance to the estimate in (Kolokotroni et al., 2011; Martínez-González et al., 2012). The work in (Toley and Forbes, 2011) provides a value for the bacterial motility coefficient and proliferation rate in *in vitro* cellular aggregates. Regarding bacterial proliferation, (Gibson et al., 2018) supply a similar value using evolutionary arguments. We estimate the bacterial death rate from (Phaiboun et al., 2015), in which cellular death dynamics are quantified under starvation at different bacteria densities. Finally, we use the values in (Schaller and Meyer-Hermann, 2005; Matzavinos et al., 2009; Grimes et al., 2014; Colombo et al., 2015; Alfonso et al., 2016) for the oxygen diffusion coefficient and consumption rate in tumor tissues. When carrying out the simulations, we vary the chemotactic coefficient in the interval $[0, 8.64 \times 10^{-1}]\,\mathrm{mm^2 d^{-1}}$. Since it was not possible to find in the literature an estimate for the chemotactic coefficient of bacteria in tissues, we considered the value of χ in bacterial solutions (Ford et al., 1991; Lewus and Ford, 2001) and divided it for the ratio between the motility coefficient in solution and in tissue - about 100, (Ford et al., 1991; Lewus and Ford, 2001). Since we do not consider a specific mechanism for the anti-tumor activity of bacteria, we select the killing rate κ to be in the interval $[0, 10]\,\mathrm{d^{-1}}$, i.e. spanning characteristic times between

bioRxiv preprint doi: https://doi.org/10.1101/683839; this version posted June 27, 2019. The copyright holder for this preprint (which was not certified by peer review) is the author/funder. All rights reserved. No reuse allowed without permission.

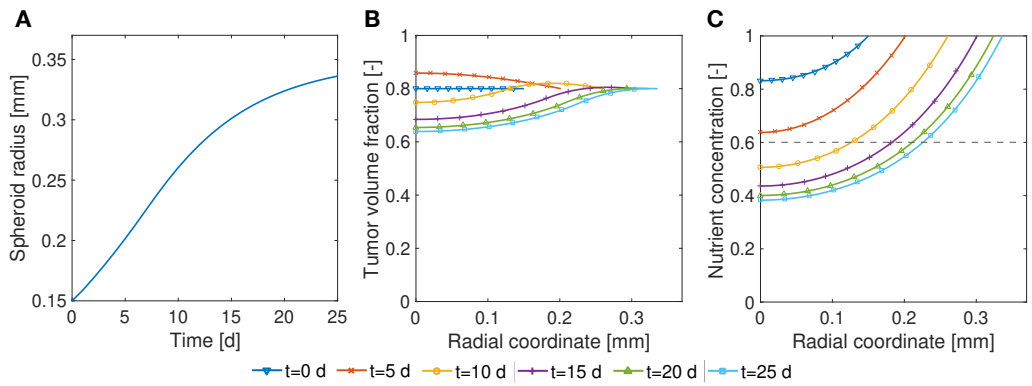

Figure 1: Spatio-temporal description of a tumor spheroid suspended in the culture medium. **A** Spheroid growth curve. Tumor volume fraction (**B**) and nutrient concentration (**C**) over the spheroid radius at different time points. The dashed line in **C** displays the critical nutrient level. After an initial stage of fast growth, the size of the aggregate saturates as a result of poor nutrient availability.

several days and a few hours.

3. Results

3.1. Growth of spheroids in culture medium

We start the analysis by considering the growth of a spheroid suspended in culture medium, in the absence of bacteria. Results for this condition are reported in Figure 1, using the parameters in Table 1 for the simulation. The model is able to reproduce the two phases of spheroid growth usually described in the literature (Conger and Ziskin, 1983; Sutherland, 1988; Vinci et al., 2012). The spheroid radius (see Figure 1**A**) displays a first stage of rapid increase, followed by a saturation phase. This behavior is detailed in Figures 1**B**,**C**, showing the evolution of the tumor volume fraction and nutrient concentration over the spheroid radius at different time points. The tumor volume fraction, i.e. ϕ_c, increases over the spheroid at early time points (Figure 1**B**). Then, as TCs consume oxygen to proliferate, its concentration decreases in the centre of the aggregate (Figure 1**C**). When the oxygen level drops below the critical threshold n_{cr} (dashed line in Figure 1**C**), TCs stop proliferating and die. This results in a decrease of ϕ_c in the spheroid core, displayed at longer times in Figure 1**B**. Close to saturation, the amount of cells that proliferate is balanced by the number of cells that die, turning into

bioRxiv preprint doi: https://doi.org/10.1101/683839; this version posted June 27, 2019. The copyright holder for this preprint (which was not certified by peer review) is the author/funder. All rights reserved. No reuse allowed without permission.

extracellular material. Therefore, even if cell growth continues to take place in the outer rim of the spheroid, it is not enough to advance the spheroid front, which reaches a steady state. These results match qualitatively what is observed in the experimental (Landry et al., 1982; Montel et al., 2011; Grimes et al., 2014; Sarkar et al., 2018) and modeling (Ward and King, 1999; Byrne and Preziosi, 2003; Ambrosi and Mollica, 2004; Schaller and Meyer-Hermann, 2005; Mascheroni et al., 2016; Boemo and Byrne, 2019) literature for tumor spheroids and will serve as a basis for the discussion in the next sections.

3.2. Spheroid growth in the presence of bacteria

In this subsection, we investigate the growth of a spheroid that is co-cultured with bacteria immediately after its formation. From the modeling point of view, this results in assuming a constant bacterial volume fraction at the spheroid boundary, i.e. $\phi_{\mathrm{b}}(R,t) = \phi_{\mathrm{b}0}$. First, we analyse the case of bacteria infiltrating the spheroid with different chemotactic coefficients χ, without considering the anti-tumor activity of bacteria (i.e. $\kappa = 0\,\mathrm{d}^{-1}$). Then, we fix the chemotactic coefficient and analyze the evolution of the spheroid for increasing effectiveness of bacteria anti-tumor activity, quantified by the killing coefficient κ.

3.2.1. Effects of chemotactic coefficient on spheroid growth

The impact of bacterial chemotactic coefficient on spheroid infiltration is shown in Figure 2. The presence of bacteria in the culture medium significantly influences the growth dynamics, as displayed by the growth curve in Figure 2**A**. For low chemotactic coefficients the saturation radius of the spheroid decreases. However, by increasing the chemotactic coefficient the growth curve loses the saturation phase (at least for the time observed in the simulation). The spheroid reaches the largest size for the highest value of χ, being still in a fast-growing regime. Figure 2**B** shows how the tumor volume fraction at the end of the simulation is affected by bacterial chemotaxis. Bacteria progressively displace TCs for increasing values of the chemotactic coefficient, leading to spheroids that are significantly depleted from TCs at higher χ values. We note that chemotaxis is necessary for bacteria to effectively colonize the core of the spheroid, as displayed by the plot of bacterial volume fraction at the end of the simulation in Figure 2**C**. Bacteria that are not subject to chemotaxis ($\chi = 0\,\mathrm{mm}^2\mathrm{d}^{-1}$) do not colonize successfully the spheroid, and populate the aggregate through a low uniform volume fraction.

bioRxiv preprint doi: https://doi.org/10.1101/683839; this version posted June 27, 2019. The copyright holder for this preprint (which was not certified by peer review) is the author/funder. All rights reserved. No reuse allowed without permission.

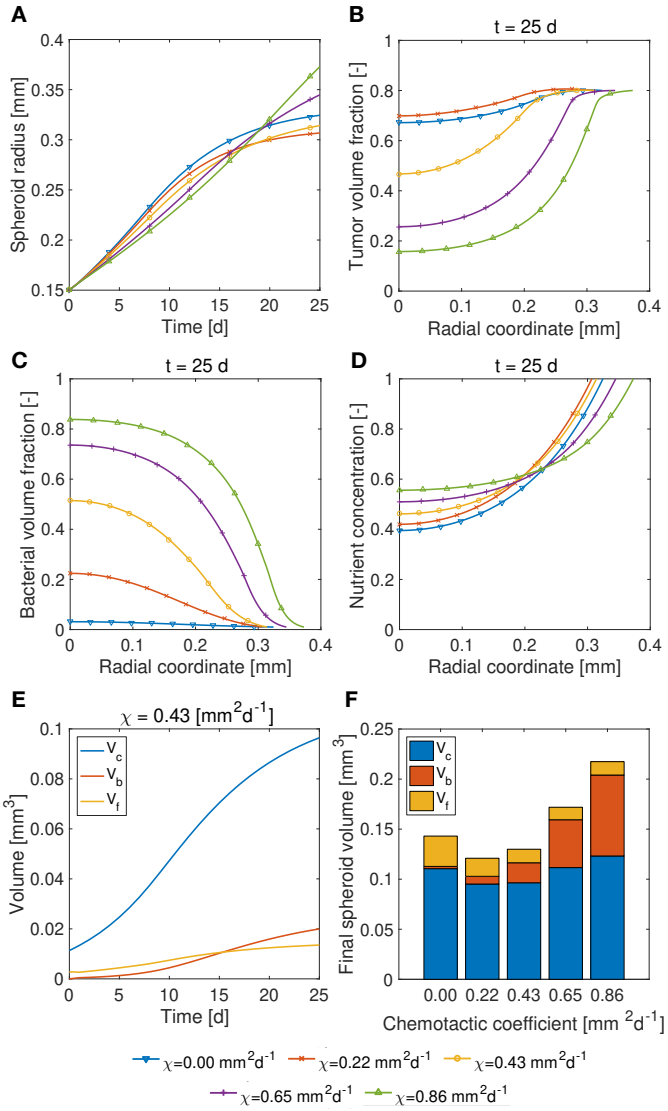

Figure 2: Influence of bacterial chemotactic coefficient on spheroid infiltration. **A** Spheroid growth over time. Profiles of tumor (**B**) and bacterial (**C**) volume fractions, and nutrient concentration (**D**) over the spheroid radius for different values of χ at the end of the simulation. **E** Variation of TC, bacterial and extracellular volumes over time for an intermediate value of χ. **F** Contribution of the different constituents to the final spheroid volume. The model shows that chemotaxis is necessary for bacteria to localize in the hypoxic core of the spheroid. Moreover, high chemotactic coefficients lead to spheroids with larger radii.

bioRxiv preprint doi: https://doi.org/10.1101/683839; this version posted June 27, 2019. The copyright holder for this preprint (which was not certified by peer review) is the author/funder. All rights reserved. No reuse allowed without permission.

On the other hand, higher values of χ lead to large bacterial volume fractions in the center of the spheroid, where a hypoxic region is localized. As a result, the core of these spheroids is filled with bacterial cells, as observed in experimental works (Osswald et al., 2015; Suh et al., 2018). Such hypoxic zones occupy most of the spheroid, as shown by the plot for the nutrient concentration over the spheroid radius (Figure 2**D**). The nutrient level generally elevates for higher values of the chemotactic coefficient, since in those cases there are fewer TCs that consume oxygen. As displayed in Figures 2**B** and 2**C**, high values of the chemotactic coefficient lead to spheroids with large final radii but low TC volume fraction in the core. The growth of bacteria pushes cancer cells towards the spheroid boundary, leading only a small fraction of them above the hypoxic threshold. Figure 2**E** shows the evolution of TC (V_c), bacterial (V_b) and extracellular (V_f) volumes over time for an intermediate chemotactic coefficient. These quantities are calculated as

$$V_\mathrm{i} = \int_{V_\mathrm{sf}} \phi_\mathrm{i}\, dV, \tag{23}$$

where the integral is performed over the spheroid volume V_sf (i = c, b, f). At early time points, V_c is in a phase of fast growth, since nutrient is available throughout the spheroid and bacterial presence is minimal. At later times, hypoxic regions develop and TC proliferation decreases. On the contrary, these conditions are favourable for bacteria, leading to a higher growth rate for V_b. The growth of both TCs and bacteria over time contributes to a slow increase of extracellular material, as displayed by the plot of V_f over time. Figure 2**F** shows the contribution of TCs, bacteria and extracellular fluid to the final spheroid volume. Note that lower volumes are attained for intermediate chemotactic coefficients ($\chi = 0.22,\ 0.43\,\mathrm{mm^2 d^{-1}}$). For these cases, bacteria compete with TCs for space and lead to low TC volumes. On the other hand, higher values of χ lead to considerable colonization of the spheroid by bacteria, contributing to higher bacterial and spheroid volumes.

3.2.2. Effects of killing rate on spheroid growth

Figure 3 shows the influence of the killing rate κ on the growth of a tumor spheroid. For these simulations, we considered an intermediate value of the chemotactic coefficient ($\chi = 0.43\,\mathrm{mm^2 d^{-1}}$), to allow for spheroid infiltration by bacteria. Increasing κ leads to significant changes in spheroid morphology. As shown in Figures 3**A**,**B** TCs display higher volume fractions for higher values of the killing coefficient, whereas the opposite is true for

bioRxiv preprint doi: https://doi.org/10.1101/683839; this version posted June 27, 2019. The copyright holder for this preprint (which was not certified by peer review) is the author/funder. All rights reserved. No reuse allowed without permission.

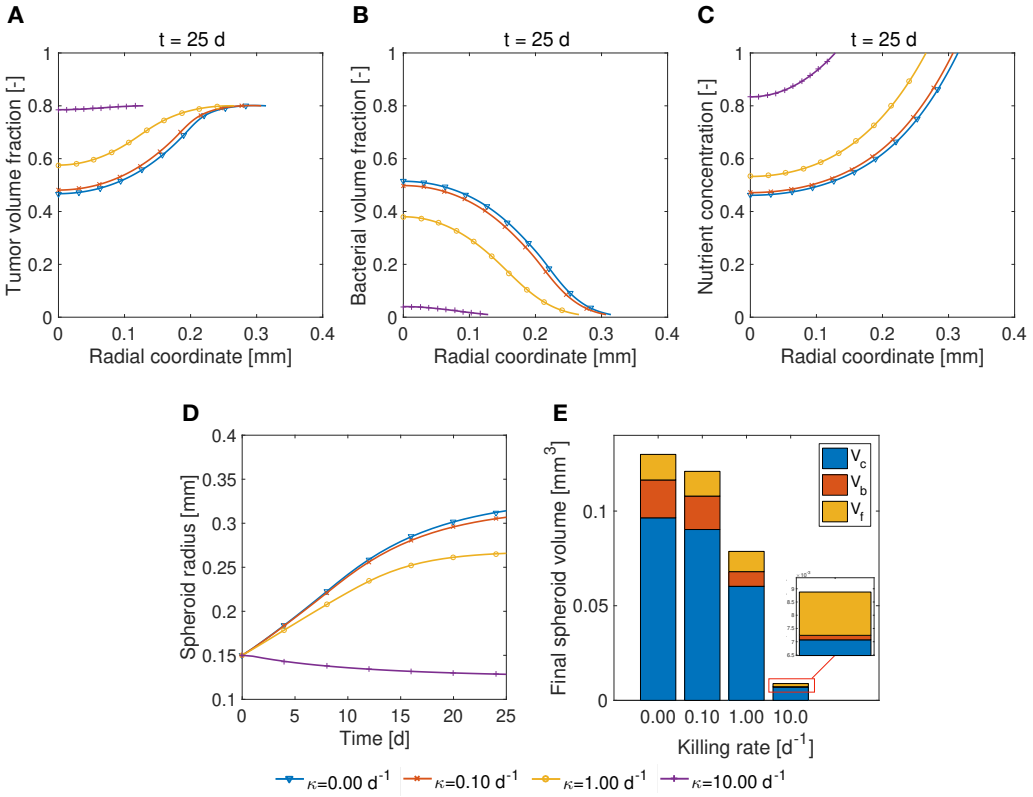

Figure 3: Influence of bacterial killing coefficient on spheroid growth. Plots of tumor (**A**) and bacterial (**B**) volume fractions, and nutrient concentration (**C**) over the spheroid radius for different values of κ at the end of the simulation. Spheroid growth curve (**D**) and contribution of the different constituents to the final spheroid volume (**E**). Increasing the killing rate leads to smaller spheroids and lower final bacterial volumes.

bioRxiv preprint doi: https://doi.org/10.1101/683839; this version posted June 27, 2019. The copyright holder for this preprint (which was not certified by peer review) is the author/funder. All rights reserved. No reuse allowed without permission.

bacteria. Consistently with the behavior of the previous quantities, nutrient concentration (Figure 3**C**) increases for higher values of κ, since smaller spheroids are formed and nutrient can adequately diffuse to their cores. The effect of the killing rate on the spheroid radius is displayed in Figure 3**D**. By increasing the value of κ, the growth rate of the spheroid decreases, turning even to negative for the highest κ value. The final volume of the spheroids decreases with increasing the cell killing rate (Figure 3**E**), a trend that is also followed by the ratio of the bacterial to TC volumes. The extracellular volume also decreases with increasing κ, indicating that spheroids denser in TCs are obtained.

3.3. Administration of bacteria to established spheroids

In this subsection, we evaluate the effects of adding bacteria in the culture medium after the spheroid is fully formed, i.e. when hypoxic regions have developed. We analyze the effects of different bacterial chemotactic and killing coefficients on the behavior of the model constituents and on the overall growth of the spheroid at later times after bacteria administration.

3.3.1. Effects of chemotactic coefficient on spheroid growth after bacterial administration

Figure 4**A** shows the growth curves of spheroids that have been administered to bacteria carrying different chemotactic coefficients. The spheroid grows in standard culture medium until day 25, when a bacterial administration (black arrow) is performed. The boundary condition $\phi_{\mathrm{b}}(R,t) = \phi_{\mathrm{b0}}$ is applied for three days and then bacteria are removed at day 28 (first dashed line). In the absence of chemotaxis ($\chi = 0\,\mathrm{mm^2d^{-1}}$) the presence of bacteria leads to a small perturbation in the growth curve, which is resolved at the end of the simulation. On the contrary non-zero values of χ substantially alter the growth pattern, resulting in spheroids of smaller (intermediate values of χ) or larger (high values of χ) final radii (Figure 4**B**).

The behavior of the different components of the model at day 28, 33 (dashed lines in Figure 5) and 53 is reported in Figure 5. TC volume fraction is considerably affected by the chemotactic behavior of bacterial cells, in all the three observation times (Figures 5**A**,**D**,**G**). Chemotactic coefficients greater than $\chi = 0.22\,\mathrm{mm^2d^{-1}}$ lead to lower ϕ_{c} at the spheroid center with respect to the no-chemotactic case ($\chi = 0\,\mathrm{mm^2d^{-1}}$). For the highest value of χ the spheroid core is mostly composed of bacteria, a situation that persists

bioRxiv preprint doi: https://doi.org/10.1101/683839; this version posted June 27, 2019. The copyright holder for this preprint (which was not certified by peer review) is the author/funder. All rights reserved. No reuse allowed without permission.

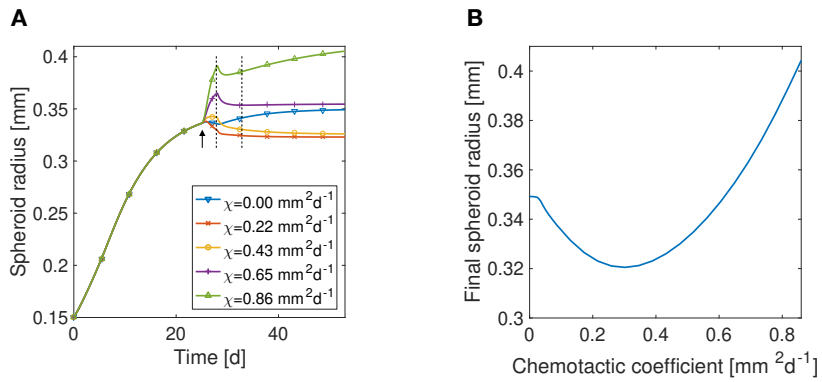

Figure 4: **A** Influence of bacterial chemotactic coefficient on tumor spheroids growth curve after bacterial administration. The black arrow indicates the time of bacterial administration, whereas the dashed lines highlight the observation time points in the following plots. Intermediate values of χ lead to smaller saturation radii if compared to bacterial infiltration in the absence of chemotaxis. On the other hand, higher chemotactic coefficients give rise to larger spheroids. **B** Final spheroid radius as a function of the chemotactic coefficient. The minimum radius is for $\chi \approx 0.3\text{mm}^2\text{d}^{-1}$.

even at 53 days, far from the administration time. Bacteria have successfully colonized the spheroid and TCs are pushed towards the outer rim of the spheroid, where oxygen is still above the critical limit. The plots for bacterial volume fraction (Figures 5**B**,**E**,**H**) clearly show that chemotaxis is necessary to allow for bacterial colonization of the spheroid. The case of $\chi = 0\,\text{mm}^2\text{d}^{-1}$, indeed, shows bacterial cells only right after the administration at day 28 (Figure 5**B**). At later time points (Figures 5**E**,**H**) the bacterial volume fraction is zero across the whole spheroid radius, indicating that bacteria have not managed to adequately infiltrate the aggregate. Regarding the other chemotactic coefficients, the plots for ϕ_b mirror those for ϕ_c, i.e. the fraction of spheroid occupied by bacteria increases with the chemotactic coefficient. Concerning the nutrient concentration, the case without chemotaxis shows the lowest nutrient level across the spheroid for all the time points (Figures 5**C**,**F**,**I**). In this case, the spheroid is almost entirely composed of TCs which consume oxygen to proliferate. As in the other conditions ($\chi \neq 0\,\text{mm}^2\text{d}^{-1}$) bacteria take the place of TCs over the spheroid radius, lower TC volume fractions lead to diminished nutrient consumption.

Finally, we consider in Figure 6 how the model components add to the spheroid volume at the different observation time points. Consistently with Figure 5 bacteria moving without chemotaxis do not contribute to the spheroid

bioRxiv preprint doi: https://doi.org/10.1101/683839; this version posted June 27, 2019. The copyright holder for this preprint (which was not certified by peer review) is the author/funder. All rights reserved. No reuse allowed without permission.

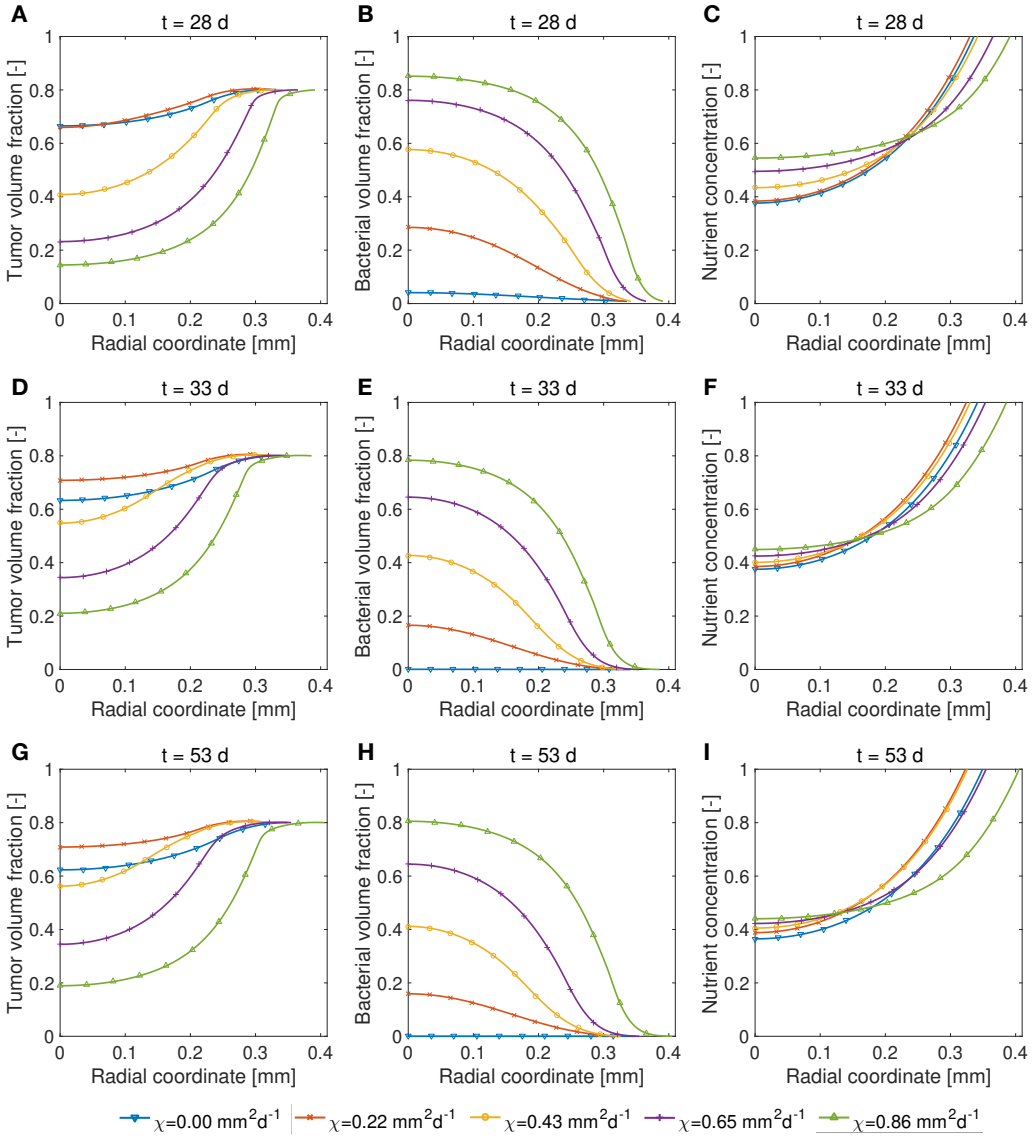

Figure 5: Plots for the volume fractions (TCs and bacteria) and nutrient concentration over the spheroid radius at different observation time points after bacterial administration. Different chemotactic coefficients are considered. TCs: **A**, **D**, **G**; bacteria: **B**, **E**, **H**; nutrient: **C**, **F**, **I**. Chemotaxis is necessary for successful colonization of the spheroid by bacteria. High values of the chemotactic coefficient lead to larger spheroids populated by high bacterial volume fractions.

bioRxiv preprint doi: https://doi.org/10.1101/683839; this version posted June 27, 2019. The copyright holder for this preprint (which was not certified by peer review) is the author/funder. All rights reserved. No reuse allowed without permission.

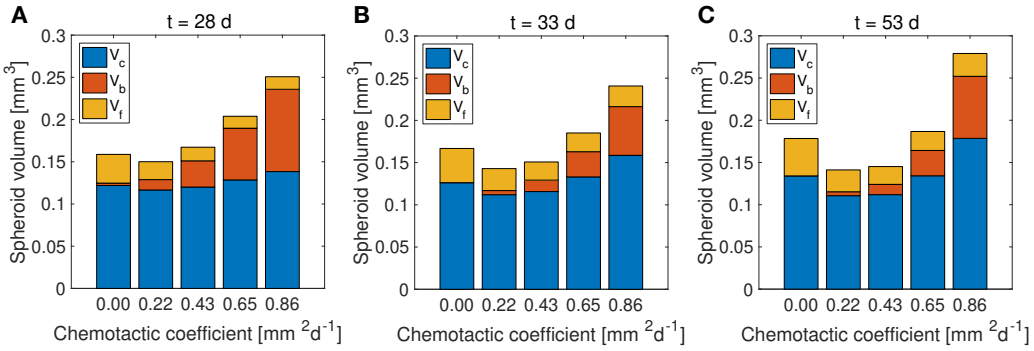

Figure 6: Composition of the spheroid volume at day 28 (**A**), 33 (**B**) and 53 (**C**) for different chemotactic coefficients in the case of bacterial administration. Intermediate chemotactic coefficients lead to smaller spheroid volumes. The fraction of bacterial volume increases with the value of the chemotactic coefficient.

volume at later time points (Figures 6**B**,**C**). Intermediate values of the chemotactic coefficient lead to small spheroid volumes, in which the bacterial volume is small if compared to the TC volume. As the value for χ increases, larger spheroids are formed, with a significant fraction of bacteria in their volume. In all the cases for which chemotaxis is present the volume of extracellular material is greater than for the case of no-chemotaxis, indicating that bacteria compete for the space of both extracellular material and TCs.

3.3.2. Effects of killing rate on spheroid growth after bacterial administration

Figure 7**A** shows the growth curves of spheroids infiltrated by bacteria characterized by different killing rates. For these simulations we allowed the bacteria to colonize the spheroid by selecting an intermediate chemotactic coefficient ($\chi = 0.43\,\mathrm{mm^2d^{-1}}$). By increasing the cell killing rate the spheroids reach decreasing saturation radii. For the highest value of the killing rate the spheroid size shows a damped oscillation that dies out approaching the end of the simulation. In Figure 7**B**, we analyze the effects of TC proliferation rate and bacterial killing rate on the number of sign changes in spheroid radial velocity (i.e. dR/dt) after bacterial administration. This quantity is correlated to the frequency of the damped oscillations that occur after bacteria are added to the culture medium. No oscillations are present for low proliferation and killing rates. For increasing γ_c and κ, however, the oscillation frequency increases. As in the previous section, we analyze the behavior of the model components at different time points after the bacterial administration, i.e.

bioRxiv preprint doi: https://doi.org/10.1101/683839; this version posted June 27, 2019. The copyright holder for this preprint (which was not certified by peer review) is the author/funder. All rights reserved. No reuse allowed without permission.

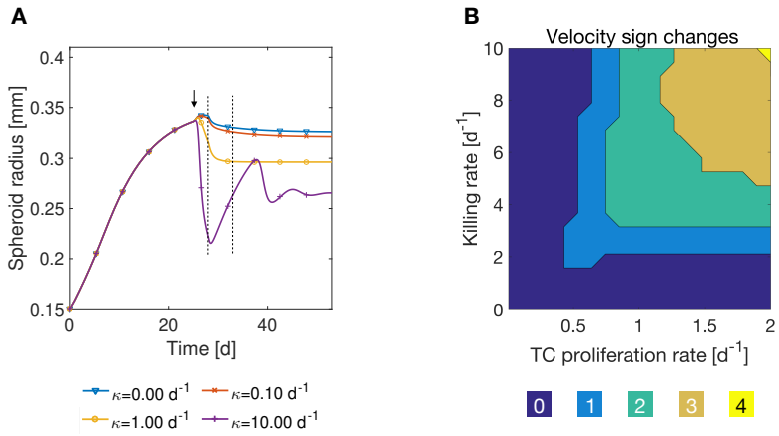

Figure 7: **A** Influence of cell killing rate on tumor spheroid growth curves after bacterial administration. The black arrow indicates the time of bacterial administration, whereas the dashed lines highlight the observation time points in the following plots. The final spheroid radius decreases with increasing cell killing rates. The highest killing rate ($\kappa = 10\,\mathrm{d}^{-1}$) gives rise to oscillations of the spheroid size, which die out at longer times. **B** Number of sign changes in spheroid radial velocity after administration, corresponding to the frequency of the oscillations in spheroid radius. The number of sign changes increases with increasing TC proliferation rate and killing rate.

at day 28, 33 (dashed lines in Figure 7) and 53 (end of the simulation).

Figure 8 provides an account of the variation of the volume fractions (of TCs and bacteria) and the nutrient concentration over the spheroid radius at the three observation times. Right after bacterial administration (day 28) the TC volume fractions are similar between the different conditions, with the exception of the highest killing rate case ($\kappa = 10\,\mathrm{d}^{-1}$). This condition leads to the smallest spheroid, characterized by the highest TC volume fraction (Figure 8**A**). At longer times after administration the differences in TC volume fraction between the various killing ratios reduce (Figures 8**D**,**G**), albeit the higher volume fractions are still obtained for the higher values of κ. The bacterial volume fraction shows a gradual decrease from higher values after administration to lower values at later time points (Figures 8**B**,**E**,**H**). A different scenario occurs for the highest killing rate case, for which the bacterial population oscillates. Starting from an observable volume fraction at day 28 (Figure 8**B**) bacteria have almost disappeared from the spheroid at day 33 (Figure 8**E**). However, at day 53 a non-zero bacterial population is still visible in Figure 8**H**; as the administration phase was concluded at

bioRxiv preprint doi: https://doi.org/10.1101/683839; this version posted June 27, 2019. The copyright holder for this preprint (which was not certified by peer review) is the author/funder. All rights reserved. No reuse allowed without permission.

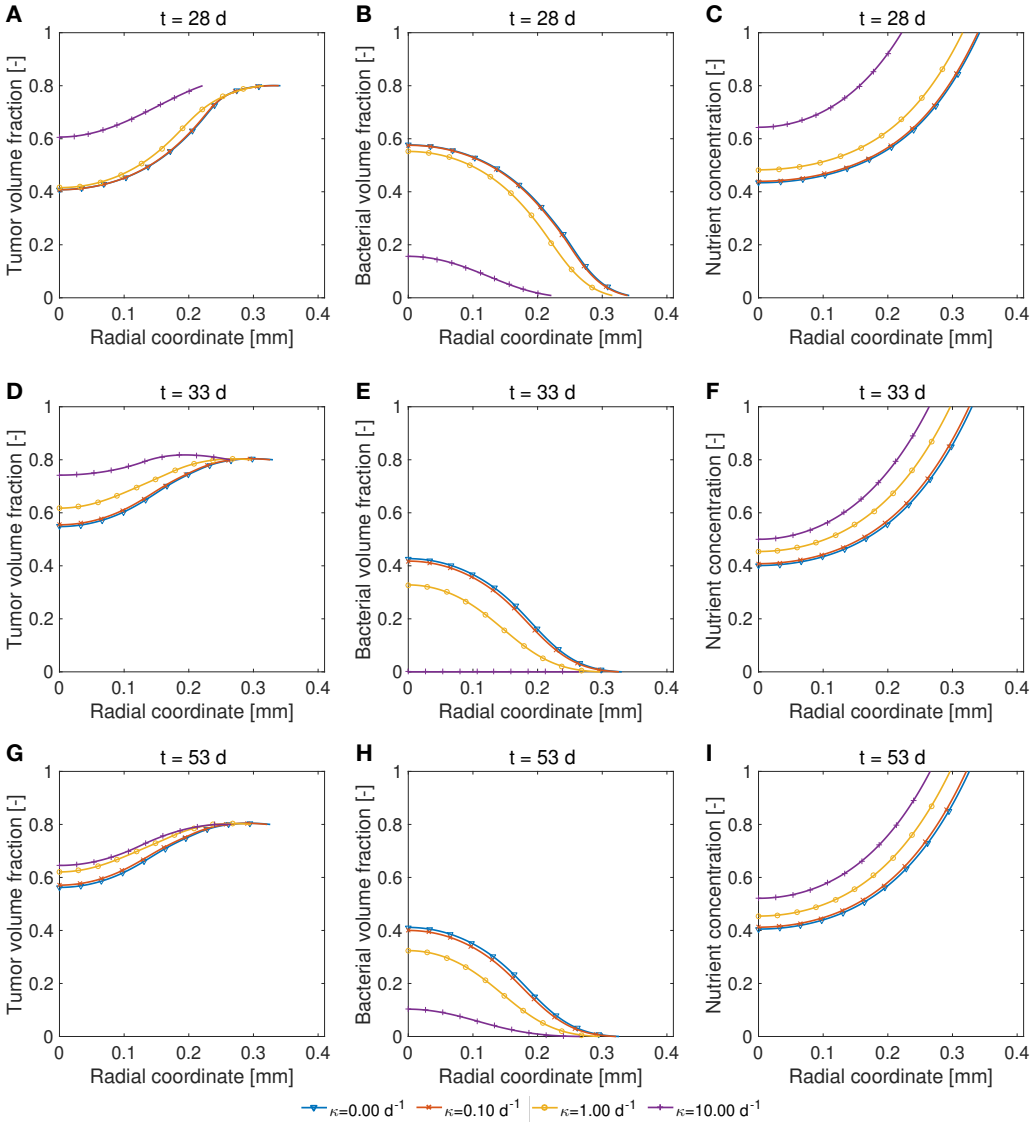

Figure 8: Plots for the volume fractions (TCs and bacteria) and nutrient concentration over the spheroid radius at different observation time points after bacterial administration. Different cell killing rates are considered. TCs: **A**, **D**, **G**; bacteria: **B**, **E**, **H**; nutrient: **C**, **F**, **I**. Increasing the killing rate leads to smaller spheroids with higher TC volume fractions in the core. Bacterial volume fractions are lower over the spheroid radius for larger values of κ, whereas the opposite occurs for nutrient concentration.

bioRxiv preprint doi: https://doi.org/10.1101/683839; this version posted June 27, 2019. The copyright holder for this preprint (which was not certified by peer review) is the author/funder. All rights reserved. No reuse allowed without permission.

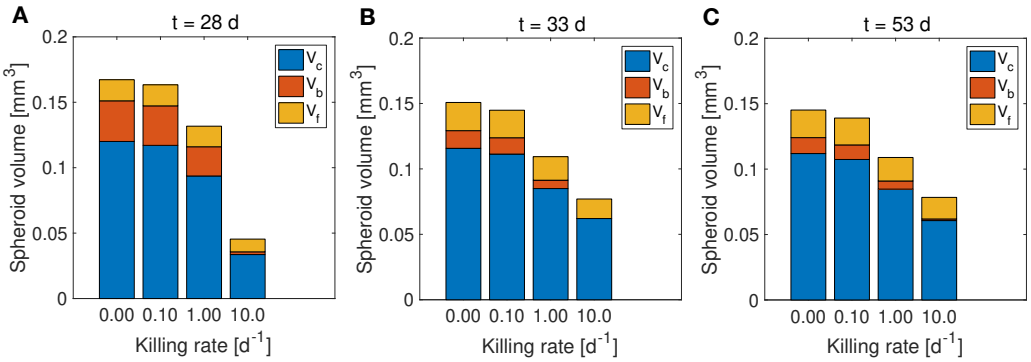

Figure 9: Composition of the spheroid volume at day 28 (**A**), 33 (**B**) and 53 (**C**) for different cell killing rates κ in the case of bacterial administration. The overall spheroid volume decreases with increasing cell killing rates. This also occurs for both TC (V_c) and bacteria (V_b) volumes, the latter showing a larger reduction with increasing values of κ.

day 28 and there are no bacteria in the culture medium, this volume fraction derives from regrowth of the surviving bacteria. The volume of bacteria, indeed, decreases at the end of bacteria administration and then increases again over time (Figure S1). Regarding the nutrient concentration, hypoxic regions are present in the spheroid at all the observation points for almost all the killing ratios (Figures 8**C**,**F**,**I**). Again, this does not occur for the case with the highest killing ratio at day 28 (Figure 8**C**), for which the nutrient level is above the critical threshold. At later times (Figures 8**F**,**I**) hypoxic regions appear also for this case, although of minor extension if compared to the other conditions.

The contribution of TCs, bacteria and extracellular material to the spheroid volume at the three observation points is shown in Figure 9. Generally the total volume of the spheroids decreases over time and for increasing values of the killing rate κ. Both the fractions of spheroid volume occupied by TCs and bacteria decrease with increasing κ, however the reduction for bacterial cells is more evident. For the highest value of κ the TC volume grows from day 28 to day 33 (Figures 9**B**,**C**) and then stabilizes at day 53 (Figure 9**C**) as a consequence of the oscillations in spheroid radius observed in Figure 7.

4. Discussion

We have adapted a continuum model for macrophage-mediated tumor treatment originally developed by Boemo and Byrne (2019) to study the

bioRxiv preprint doi: https://doi.org/10.1101/683839; this version posted June 27, 2019. The copyright holder for this preprint (which was not certified by peer review) is the author/funder. All rights reserved. No reuse allowed without permission.

influence of bacteria on avascular tumor growth. We considered anaerobic bacteria which thrive in hypoxic environments and actively migrate towards nutrient deprived regions in solid tumors. We applied the model to tumor spheroids and tested the impact of bacteria chemotaxis and killing rate on spheroid dynamics. In our analysis, we considered both continuous infusion and time-dependent administration of bacteria in the culture medium. We found that chemotaxis is necessary for successful tumor infiltration, as only for non-zero values of the chemotactic coefficient bacteria were able to colonize the inner regions of the spheroid. Model results also showed that the best treatment effect in terms of minimum spheroid size is obtained at intermediate values of the chemotactic coefficient, and that spheroid volume increases for increasing chemotaxis strength. Next, we considered the impact of the effective rate at which bacteria perform an anti-tumor activity on the cancer cells. As expected, increasing the killing rate at an intermediate chemotactic coefficient reduces the total spheroid size. However, the ratio between the fraction of spheroid volume occupied by bacteria to TCs also decreases, suggesting that bacteria are not able to support their own survival by exerting an anti-tumor activity on TCs. In the case of time-dependent administration of bacteria, the model predicted the onset of oscillations in the spheroid volume. These oscillations occur only for high TC proliferation and bacterial killing rates, with a frequency that increases for increasing values of the latter parameters.

For simplicity, we considered a general effective anti-tumor activity of TCs by bacteria without focusing on specific mechanisms, e.g. cytotoxic agents, prodrug-converting enzymes, etc. (Torres et al., 2018; Zhou et al., 2018; Kramer et al., 2018). Such treatment modalities could be incorporated by extending the model, to provide a more accurate description of the therapeutic action. Moreover, we focused on tumor spheroids, an *in vitro* approximation of avascular tumors. As such, they lack all the interactions between the tumor and its immune environment. Including the cross-talk between bacteria and the components of the immune system would be a fundamental step to address questions coming from *in vivo* tumors. We modeled the mechanical response of cells and bacteria in the simplest way, considering the phases as inviscid fluids. Although this description is still able to qualitatively describe the experimental results, more detailed constitutive assumptions for the mechanical behavior of the phases would lead to new insights into the interactions between bacteria and TCs in the aggregate (Sciumè et al., 2013; Giverso et al., 2015; Ambrosi et al., 2017; Mascheroni

bioRxiv preprint doi: https://doi.org/10.1101/683839; this version posted June 27, 2019. The copyright holder for this preprint (which was not certified by peer review) is the author/funder. All rights reserved. No reuse allowed without permission.

et al., 2018; Fraldi and Carotenuto, 2018; Giverso and Preziosi, 2019). We also considered ideal spherical spheroids to reduce the mathematical problem to one dimension. Even if the qualitative results will be maintained in a three-dimensional geometry, adopting the latter will be crucial to translate the model to *in vivo* situations.

In this modeling approach, space competition between bacteria and tumor cells arises naturally from the conservation of mass and momentum imposed by the governing equations. As no void regions are allowed into the spheroid, when cells move or die one of the model components automatically fills the space. At intermediate chemotaxis levels, bacteria and TCs compete for space in the spheroid core and the expansion of TCs becomes limited. In this condition, indeed, we find the lowest fractions of TCs and bacteria in the spheroid volume. On the other hand, for increasing values of the chemotactic coefficient, bacteria localize predominantly in the spheroid core and displace TCs to the outer region of the spheroid. Both types of cell can proliferate in each of the two spheroid areas (hypoxic for spheroids, well-oxygenated for TCs), giving rise to high fractions of TCs and bacteria in the overall spheroid volume. As a matter of fact, chemotaxis could be a target for bacteria-based anticancer therapies. This mechanism arises as a pure physical effect from the competition for space and nutrients between cancer and bacteria cells and could be optimized to obtain the highest tumor volume reduction. Currently, even though researchers are aware of the benefits coming from active bacteria migration towards hypoxic regions in tumors (Forbes, 2010; Kramer et al., 2018), this knowledge has not been efficiently exploited in the clinical trials carried out so far (Torres et al., 2018).

Since bacteria thrive in hypoxic conditions, removal of TCs improves oxygenation of the spheroid, which leads to less favourable conditions for bacterial cells. Better oxygenation of the spheroids could also be exploited to improve the sensitivity of cancer cells to standard chemotherapies, in the context of synergistic treatments (Zhou et al., 2018). In (Owen et al., 2004), the authors noted a similar effect when modeling macrophages in spheroids, another example showing that mathematical models could help identifying situations when TC sensitization to therapies might be possible - see also (Kim et al., 2013; Michor and Beal, 2015; Mascheroni et al., 2017).

Finally, we point out two straightforward developments that emerge from the findings of this work. First, one could think about extending the model to consider different bacterial administration schedules. The duration of bacteria administration, the time of administration and single vs. multiple

bioRxiv preprint doi: https://doi.org/10.1101/683839; this version posted June 27, 2019. The copyright holder for this preprint (which was not certified by peer review) is the author/funder. All rights reserved. No reuse allowed without permission.

dosing could be investigated to determine the optimal conditions for this kind of treatment. Secondly, the tight coupling between the dynamics of TCs and bacteria in terms of regulating their reciprocal environment could be addressed via mathematical models, in order to control the bacterial infection or identify the optimal timing of the therapy.

Acknowledgements

M.M.H. and H.H. gratefully acknowledge the funding support of the Helmholtz Association of German Research Centers - Initiative and Networking Fund for the project on Reduced Complexity Models (ZT-I-0010). H.H. and P.M. acknowledge the funding support of MicMode-I2T (01ZX1710B) by the Federal Ministry of Education and Research (BMBF).

References

Agosti, A., Cattaneo, C., Giverso, C., Ambrosi, D., Ciarletta, P., 2018. A computational framework for the personalized clinical treatment of glioblastoma multiforme. ZAMM-Journal of Applied Mathematics and Mechanics/Zeitschrift für Angewandte Mathematik und Mechanik 98 (12), 2307–2327.

Alfonso, J., Köhn-Luque, A., Stylianopoulos, T., Feuerhake, F., Deutsch, A., Hatzikirou, H., 2016. Why one-size-fits-all vaso-modulatory interventions fail to control glioma invasion: in silico insights. Scientific reports 6, 37283.

Altrock, P. M., Liu, L. L., Michor, F., 2015. The mathematics of cancer: integrating quantitative models. Nature Reviews Cancer 15 (12), 730.

Ambrosi, D., Mollica, F., 2004. The role of stress in the growth of a multicell spheroid. Journal of mathematical biology 48 (5), 477–499.

Ambrosi, D., Pezzuto, S., Riccobelli, D., Stylianopoulos, T., Ciarletta, P., 2017. Solid tumors are poroelastic solids with a chemo-mechanical feedback on growth. Journal of Elasticity 129 (1-2), 107–124.

Ambrosi, D., Preziosi, L., 2002. On the closure of mass balance models for tumor growth. Mathematical Models and Methods in Applied Sciences 12 (05), 737–754.

bioRxiv preprint doi: https://doi.org/10.1101/683839; this version posted June 27, 2019. The copyright holder for this preprint (which was not certified by peer review) is the author/funder. All rights reserved. No reuse allowed without permission.

Boemo, M. A., Byrne, H. M., 2019. Mathematical modelling of a hypoxia-regulated oncolytic virus delivered by tumour-associated macrophages. Journal of Theoretical Biology 461, 102–116.

Breward, C., Byrne, H., Lewis, C., 2001. Modelling the interactions between tumour cells and a blood vessel in a microenvironment within a vascular tumour. European Journal of Applied Mathematics 12 (5), 529–556.

Breward, C., Byrne, H., Lewis, C., 2002. The role of cell-cell interactions in a two-phase model for avascular tumour growth. Journal of Mathematical Biology 45 (2), 125–152.

Breward, C. J., Byrne, H. M., Lewis, C. E., 2003. A multiphase model describing vascular tumour growth. Bulletin of mathematical biology 65 (4), 609–640.

Byrne, H., 2012. Mathematics and life sciences.

Byrne, H., Preziosi, L., 2003. Modelling solid tumour growth using the theory of mixtures. Mathematical medicine and biology: a journal of the IMA 20 (4), 341–366.

Byrne, H. M., 2010. Dissecting cancer through mathematics: from the cell to the animal model. Nature Reviews Cancer 10 (3), 221.

Carmeliet, P., Jain, R. K., 2000. Angiogenesis in cancer and other diseases. nature 407 (6801), 249.

Challapalli, A., Carroll, L., Aboagye, E. O., 2017. Molecular mechanisms of hypoxia in cancer. Clinical and translational imaging 5 (3), 225–253.

Chaplain, M. A., Graziano, L., Preziosi, L., 2006. Mathematical modelling of the loss of tissue compression responsiveness and its role in solid tumour development. Mathematical medicine and biology: a journal of the IMA 23 (3), 197–229.

Colombo, M. C., Giverso, C., Faggiano, E., Boffano, C., Acerbi, F., Ciarletta, P., 2015. Towards the personalized treatment of glioblastoma: integrating patient-specific clinical data in a continuous mechanical model. PLoS One 10 (7), e0132887.

bioRxiv preprint doi: https://doi.org/10.1101/683839; this version posted June 27, 2019. The copyright holder for this preprint (which was not certified by peer review) is the author/funder. All rights reserved. No reuse allowed without permission.

Conger, A. D., Ziskin, M. C., 1983. Growth of mammalian multicellular tumor spheroids. Cancer Research 43 (2), 556–560.

Folkman, J., 1971. Tumor angiogenesis: therapeutic implications. New england journal of medicine 285 (21), 1182–1186.

Forbes, N. S., 2010. Engineering the perfect (bacterial) cancer therapy. Nature Reviews Cancer 10 (11), 785.

Ford, R. M., Phillips, B. R., Quinn, J. A., Lauffenburger, D. A., 1991. Measurement of bacterial random motility and chemotaxis coefficients: I. stopped-flow diffusion chamber assay. Biotechnology and bioengineering 37 (7), 647–660.

Fraldi, M., Carotenuto, A. R., 2018. Cells competition in tumor growth poroelasticity. Journal of the Mechanics and Physics of Solids 112, 345–367.

Gerlee, P., Anderson, A. R., 2007. An evolutionary hybrid cellular automaton model of solid tumour growth. Journal of theoretical biology 246 (4), 583–603.

Gibson, B., Wilson, D. J., Feil, E., Eyre-Walker, A., 2018. The distribution of bacterial doubling times in the wild. Proceedings of the Royal Society B: Biological Sciences 285 (1880), 20180789.

Giverso, C., Preziosi, L., 2019. Influence of the mechanical properties of the necrotic core on the growth and remodelling of tumour spheroids. International Journal of Non-Linear Mechanics 108, 20–32.

Giverso, C., Scianna, M., Grillo, A., 2015. Growing avascular tumours as elasto-plastic bodies by the theory of evolving natural configurations. Mechanics Research Communications 68, 31–39.

Grimes, D. R., Kelly, C., Bloch, K., Partridge, M., 2014. A method for estimating the oxygen consumption rate in multicellular tumour spheroids. Journal of The Royal Society Interface 11 (92), 20131124.

Hanahan, D., Weinberg, R. A., 2011. Hallmarks of cancer: the next generation. cell 144 (5), 646–674.

bioRxiv preprint doi: https://doi.org/10.1101/683839; this version posted June 27, 2019. The copyright holder for this preprint (which was not certified by peer review) is the author/funder. All rights reserved. No reuse allowed without permission.

Hatzikirou, H., Alfonso, J. C. L., Leschner, S., Weiss, S., Meyer-Hermann, M., 2017. Therapeutic potential of bacteria against solid tumors. Cancer research 77 (7), 1553–1563.

Jean, A. T. S., Swofford, C. A., Panteli, J. T., Brentzel, Z. J., Forbes, N. S., 2014. Bacterial delivery of staphylococcus aureus α-hemolysin causes regression and necrosis in murine tumors. Molecular Therapy 22 (7), 1266–1274.

Kasinskas, R. W., Forbes, N. S., 2006. Salmonella typhimurium specifically chemotax and proliferate in heterogeneous tumor tissue in vitro. Biotechnology and bioengineering 94 (4), 710–721.

Kim, M., Gillies, R. J., Rejniak, K. A., 2013. Current advances in mathematical modeling of anti-cancer drug penetration into tumor tissues. Frontiers in oncology 3, 278.

Kolokotroni, E. A., Dionysiou, D. D., Uzunoglu, N. K., Stamatakos, G. S., 2011. Studying the growth kinetics of untreated clinical tumors by using an advanced discrete simulation model. Mathematical and Computer Modelling 54 (9-10), 1989–2006.

Kramer, M. G., Masner, M., Ferreira, F. A., Hoffman, R. M., 2018. Bacterial therapy of cancer: Promises, limitations, and insights for future directions. Frontiers in Microbiology 9, 16.

Landry, J., Freyer, J., Sutherland, R., 1982. A model for the growth of multicellular spheroids. Cell Proliferation 15 (6), 585–594.

Lewus, P., Ford, R. M., 2001. Quantification of random motility and chemotaxis bacterial transport coefficients using individual-cell and population-scale assays. Biotechnology and bioengineering 75 (3), 292–304.

Martínez-González, A., Calvo, G. F., Romasanta, L. A. P., Pérez-García, V. M., 2012. Hypoxic cell waves around necrotic cores in glioblastoma: a biomathematical model and its therapeutic implications. Bulletin of mathematical biology 74 (12), 2875–2896.

Mascheroni, P., Boso, D., Preziosi, L., Schrefler, B. A., 2017. Evaluating the influence of mechanical stress on anticancer treatments through a multiphase porous media model. Journal of theoretical biology 421, 179–188.

bioRxiv preprint doi: https://doi.org/10.1101/683839; this version posted June 27, 2019. The copyright holder for this preprint (which was not certified by peer review) is the author/funder. All rights reserved. No reuse allowed without permission.

Mascheroni, P., Carfagna, M., Grillo, A., Boso, D., Schrefler, B., 2018. An avascular tumor growth model based on porous media mechanics and evolving natural states. Mathematics and Mechanics of Solids 23 (4), 686–712.

Mascheroni, P., Stigliano, C., Carfagna, M., Boso, D. P., Preziosi, L., Decuzzi, P., Schrefler, B. A., 2016. Predicting the growth of glioblastoma multiforme spheroids using a multiphase porous media model. Biomechanics and modeling in mechanobiology 15 (5), 1215–1228.

Matzavinos, A., Kao, C.-Y., Green, J. E. F., Sutradhar, A., Miller, M., Friedman, A., 2009. Modeling oxygen transport in surgical tissue transfer. Proceedings of the National Academy of Sciences 106 (29), 12091–12096.

Michor, F., Beal, K., 2015. Improving cancer treatment via mathematical modeling: surmounting the challenges is worth the effort. Cell 163 (5), 1059–1063.

Montel, F., Delarue, M., Elgeti, J., Malaquin, L., Basan, M., Risler, T., Cabane, B., Vignjevic, D., Prost, J., Cappello, G., et al., 2011. Stress clamp experiments on multicellular tumor spheroids. Physical review letters 107 (18), 188102.

Osswald, A., Sun, Z., Grimm, V., Ampem, G., Riegel, K., Westendorf, A. M., Sommergruber, W., Otte, K., Dürre, P., Riedel, C. U., 2015. Three-dimensional tumor spheroids for in vitro analysis of bacteria as gene delivery vectors in tumor therapy. Microbial cell factories 14 (1), 199.

Owen, M. R., Byrne, H. M., Lewis, C. E., 2004. Mathematical modelling of the use of macrophages as vehicles for drug delivery to hypoxic tumour sites. Journal of theoretical biology 226 (4), 377–391.

Pesavento, F., Schrefler, B. A., Sciumè, G., 2017. Multiphase flow in deforming porous media: a review. Archives of Computational Methods in Engineering 24 (2), 423–448.

Phaiboun, A., Zhang, Y., Park, B., Kim, M., 2015. Survival kinetics of starving bacteria is biphasic and density-dependent. PLoS computational biology 11 (4), e1004198.

Preziosi, L., 2003. Cancer modelling and simulation. CRC Press.

bioRxiv preprint doi: https://doi.org/10.1101/683839; this version posted June 27, 2019. The copyright holder for this preprint (which was not certified by peer review) is the author/funder. All rights reserved. No reuse allowed without permission.

Preziosi, L., Tosin, A., 2009. Multiphase modelling of tumour growth and extracellular matrix interaction: mathematical tools and applications. Journal of mathematical biology 58 (4-5), 625.

Sarkar, S., Peng, C.-C., Kuo, C. W., Chueh, D.-Y., Wu, H.-M., Liu, Y.-H., Chen, P., Tung, Y.-C., 2018. Study of oxygen tension variation within live tumor spheroids using microfluidic devices and multi-photon laser scanning microscopy. RSC Advances 8 (53), 30320–30329.

Schaller, G., Meyer-Hermann, M., 2005. Multicellular tumor spheroid in an off-lattice voronoi-delaunay cell model. Physical Review E 71 (5), 051910.

Sciumè, G., Shelton, S., Gray, W. G., Miller, C. T., Hussain, F., Ferrari, M., Decuzzi, P., Schrefler, B., 2013. A multiphase model for three-dimensional tumor growth. New journal of physics 15 (1), 015005.

Siddique, J., Ahmed, A., Aziz, A., Khalique, C., 2017. A review of mixture theory for deformable porous media and applications. Applied Sciences 7 (9), 917.

Suh, S., Leaman, E., Zhan, Y., Behkam, B., 2018. Mathematical modeling of bacteria-enabled drug delivery system penetration into multicellular tumor spheroids. In: 2018 40th Annual International Conference of the IEEE Engineering in Medicine and Biology Society (EMBC). IEEE, pp. 6162–6165.

Sutherland, R. M., 1988. Cell and environment interactions in tumor microregions: the multicell spheroid model. Science 240 (4849), 177–184.

Toley, B. J., Forbes, N. S., 2011. Motility is critical for effective distribution and accumulation of bacteria in tumor tissue. Integrative Biology 4 (2), 165–176.

Torres, W., Lameda, V., Olivar, L. C., Navarro, C., Fuenmayor, J., Pérez, A., Mindiola, A., Rojas, M., Martínez, M. S., Velasco, M., et al., 2018. Bacteria in cancer therapy: beyond immunostimulation. J Cancer Metastasis Treat 4, 4.

Vaupel, P., Mayer, A., 2007. Hypoxia in cancer: significance and impact on clinical outcome. Cancer and Metastasis Reviews 26 (2), 225–239.

bioRxiv preprint doi: https://doi.org/10.1101/683839; this version posted June 27, 2019. The copyright holder for this preprint (which was not certified by peer review) is the author/funder. All rights reserved. No reuse allowed without permission.

Vinci, M., Gowan, S., Boxall, F., Patterson, L., Zimmermann, M., Lomas, C., Mendiola, M., Hardisson, D., Eccles, S. A., et al., 2012. Advances in establishment and analysis of three-dimensional tumor spheroid-based functional assays for target validation and drug evaluation. BMC biology 10 (1), 29.

Ward, J., King, J., 1999. Mathematical modelling of avascular-tumour growth ii: modelling growth saturation. Mathematical Medicine and Biology: A Journal of the IMA 16 (2), 171–211.

Wilson, W. R., Hay, M. P., 2011. Targeting hypoxia in cancer therapy. Nature Reviews Cancer 11 (6), 393.

Zhou, S., Gravekamp, C., Bermudes, D., Liu, K., 2018. Tumour-targeting bacteria engineered to fight cancer. Nature Reviews Cancer, 1.